Ti-2007 Science and Technology, edited by M. Ninomi, S. Akiyama, M. Ikeda, M. Hagiwara, K. Maruyama
The Japan Institute of Metals (2007)

The Evolution of Lattice Strain in Ti-10V-2Fe-3Al during Tensile Loading at Room Temperature

Seema Raghunathan, Adam Stapleton, Richard Dashwood, Martin Jackson, David Dye

Imperial College London, Department of Materials, South Kensington Campus, London SW7 2AZ, UK

The lattice strain evolution in near-β Ti-10V-2Fe-3Al during room temperature tensile loading has been characterised in the as-forged and forged and aged conditions using *in-situ* synchrotron X-ray diffraction. The behaviour has been modelled using a 2-phase elastic-plastic self-consistent (EPSC) model. It is found that the constrained β phase E_{200} increases from 45GPa in the as-forged condition to 88GPa in the forged-and-aged material. C_{11} — C_{12} increases from 12 to 47 GPa, due to the increase in β-stabiliser content, in agreement with atomistic predictions. The EPSC models are reasonably successful at reproducing the observed behaviour, but do not provide a complete description of the micromechanics of these materials.

Keywords: *Beta Ti Alloys, X-ray diffraction, elastic constants, micromechanics*

1. Introduction

The near-β titanium alloy, Ti-10V-2Fe-3Al(Ti-10-2-3), is used primarily in forgings for aircraft structural applications such as landing gear. It is generally observed that near-β alloys are strengthened by a fine scale dispersion of α phase precipitates developed during aging[1] which reinforce the β phase.

The self-consistent approach of Eshelby[2-3] has recently been applied[4-6] with great success to understand the load partitioning between grains in different orientations in single-phase materials. Similar models have been produced for two-phase materials, such as the nickel superalloy Waspaloy[7] but in general two-phase interactions have not been treated using this approach. However, given the success of the approach in modelling single phase materials, and in view of its computational simplicity, modelling two-phase interactions in a similar manner is attractive.

In this paper, measurements of the load partitioning between phases and grain orientations in both as-forged and forged and aged Ti-10-2-3 are presented. These measurements were obtained using *in-situ* synchrotron X-ray diffraction. A two-phase micromechanical (self-consistent) model is used to rationalise the results, together with microscopic examination of the material in the two conditions.

2. Experimental Description

α+β forged Timetal-10-2-3 was obtained from QinetiQ, Farnborough, UK. The samples were heat treated in the β phase field at 820°C for 30 minutes and then α+β forged at 760°C using the double truncated cone specimen geometry[8] at the US Air Force Research Laboratory, Dayton, OH, USA. Blocks were then removed from the forging at the central, highest strain location that experienced a primarily uniaxial strain. One of these blocks was then solution treated at 760°C and then aged at 500°C for 8 hours. Tensile specimens were then removed from both as-forged and aged blocks for testing. Backscattered electron images of the samples were obtained using a LEO Field Emission Gun Scanning Electron Microscope.

The tensile samples were mechanically tested to failure using the FaME38 Electro-thermomechanical tester on the ID11 beamline at the ESRF, Grenoble, France, using an X-ray energy of 80keV at a nominal strain rate of 10^{-4} s^{-1}. The experimental setup, Figure 1, shows the FreLoN area detector at a sample-detector distance of 256 mm used to sample the diffraction rings. Sampling times were ~ 0.5 s.

The X-ray diffraction rings were segmented and intensity-2θ diffraction profiles obtained from a 10° region corresponding to each of the longitudinal and transverse straining directions using FIT2D. The instrumental parameters were obtained using a LaB_6 powder standard. Gaussian peak fits to each diffraction peak were then performed using the Wavemetrics program Igor and an adapted version of a multi-peak fitting script written by S.S. Babu, ORNL, TN, USA.

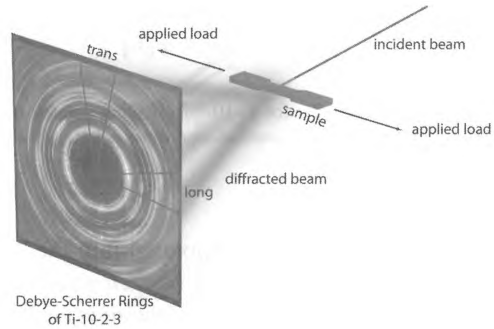

Figure 1. Schematic diagram of experimental set-up showing the specimen, incident x-ray beam and resultant diffraction rings at the detector.

d-spacings for each of the non-overlapping peaks were obtained from the spectra in each direction, Figure 2. The average elastic strain in a given direction was determine for grains satisfying the diffraction condition for a single peak *hkl* by finding the lattice parameter d^{hkl} from Bragg's Law, $\lambda = 2d \sin\theta$, relative to the unstrained, reference, lattice parameter d_0^{hkl}, as follows

$$\varepsilon^{hkl} = \Delta d^{hkl} / d_0^{hkl} \qquad (1)$$

3. Self-Consistent Modelling

The elasto-plastic self-consistent (EPSC) modelling scheme is based on the Eshelby[2] equivalent inclusion formalism and has been described elsewhere[9]. This single phase EPSC code has been rewritten in C++ and adapted to model two phase polycrystalline materials. The self-consistent stiffness is found from a linear combination of the self-consistent stiffnesses of each phase *i*, weighted by the volume fraction of each phase, w_i

$$\begin{aligned} C &= w_1 C^{sc(1)} + w_2 C^{sc(2)} \\ &= w_1 \left\langle C^{c(1)} A^{c(1)} \right\rangle + w_2 \left\langle C^{c(2)} A^{c(2)} \right\rangle \end{aligned} \qquad (2)$$

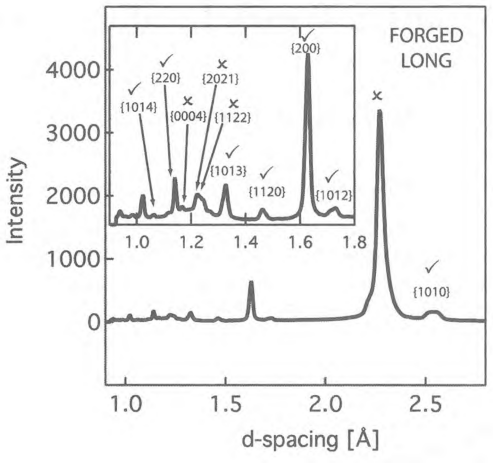

Figure 2. Intensity *vs* d-spacing for Ti-10-2-3 showing the α and β peaks. Peaks marked with a tick symbol were chosen for further analysis.

The two phase theory is incorporated into the working model by calculating the properties of each phase independently and then combining them into the the calculation of the self-consistent stiffness. If plasticity is to be considered, then Hill's [10] single crystal plasticity must be incorporated to give the C^C term.

3.1 Application to Ti-10-2-3

The forged (F) and the aged (A) cases were run using different volume fractions for each of the phases. The volume fraction of primary α for the forged material, determined from the backscattered image using UTHSCSA ImageTool, was ~ 15%. For the aged condition it was found to be ~20%. Any additional secondary a not observed using backscattered electron imaging was not directly modelled.

The single crystal elastic constants (SECs) of pure β and pure α Ti were obtained from the literature[11-12] and are detailed in Table 1. These were used as an initial estimate for the model to predict the diffraction elastic constants (DECs) for each plane. The α SECs used are listed in Table 1. There are considerable differences in the β SECs from the literature. The intrinsic problem being that the martensitic transformation prevents retention of pure β phase at room temperature after quenching. For these reasons the β phase SECs were treated as fitting parameters and adjusted until a reasonably good agreement with the experimental data was reached. The final values used in the model can be found in Table 2.

Table 1. Single crystal elastic constants (in GPa) for the α phase showing literature values as well as those used in the forged and aged computations.

	C_{11}	C_{12}	C_{13}	C_{33}	C_{44}
Smithells[12]	168.0	94.5	69.3	190.5	48.8
Forged Model	163.0	114.0	69.3	191.0	38.0
Aged Model	163.0	114.0	69.3	191.0	38.0

For the β phase, the {110}<111>, {112}<111> and {123}<111> slip modes were applied. The α phase deforms by basal, prismatic and pyramidal slip. The critical resolved shear stresses (CRSS) for each slip mode were

Table 2. Single crystal elastic constants (in GPa) for the β phase. Data is shown for both the literature (pure β-Ti) as well as the parameters used in the models.

	C_{11}	C_{12}	C_{44}	$(C_{11}-C_{12})$
Petry *et al.*[11]	134.0	110.0	36.0	24.0
Fisher & Dever[13]	99.0	85.0	33.6	14.0
Ledbetter *et al.*[14]	99.7	82.7	37.5	17.0
Forged Model	140.0	128.0	50.0	12.0
Aged Model	165.0	118.0	45.0	47.0

Table 3. CRSSs (GPa) for the α and β phases in the models.

Slip Mode	CRSS (τ_0)	
	Forged	Aged
$\alpha\{0002\}\langle 11\bar{2}0\rangle$	0.35	0.45
$\alpha\{10\bar{1}0\}\langle 11\bar{2}0\rangle$	0.17	0.42
$\alpha\{10\bar{1}1\}\langle 11\bar{2}0\rangle$	0.55	0.65
$\alpha\{11\bar{2}2\}\langle 11\bar{2}3\rangle$	0.60	0.75
$\alpha\{10\bar{1}\bar{1}\}\langle 11\bar{2}3\rangle$	0.75	0.80
$\beta\{110\}\langle 111\rangle$	0.22	0.48
$\beta\{112\}\langle 111\rangle$	0.24	0.48
$\beta\{123\}\langle 111\rangle$	0.26	0.50

chosen to give the best approximation to the bulk stress-strain curve, Table 3. Since Ti-10-2-3 contains sufficient Al to suppress twinning[15] of the α phase, $< c + a >$ slip systems were used instead, with higher critical resolved shear stresses.

4. Results & Analysis

4.1 Tensile Testing, Texture & Microstructure

The macroscopic true stress-true strain curves for the forged and aged conditions are shown in Figure 3. The forged sample behaves in an elastic manner until it yields at ~750MPa, after which point the flow stress remains constant until failure at about 9% total strain. The aged sample yields at higher stress of ~1150MPa and proceeds to soften in the plastic regime until failure occurs at ~7%. Both tests were carried out with periodic unloading and reloading.

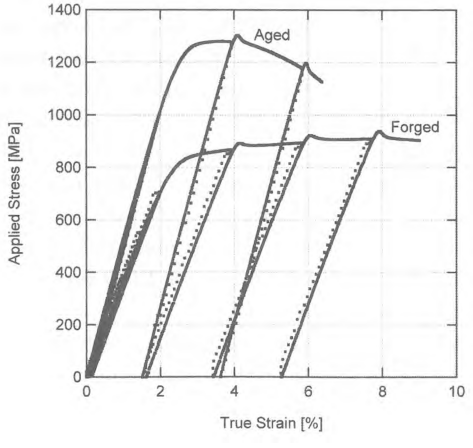

Figure 3. Macroscopic stress *vs* strain for Ti-10-2-3 under tensile loading conditions at room temperature showing both the forged and aged conditions.

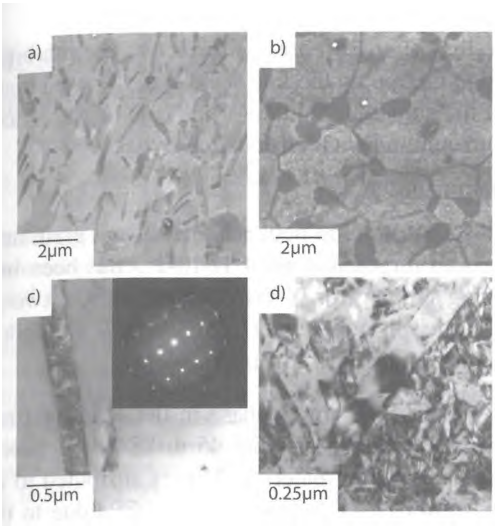

Figure 4. Microstructure of Ti-10-2-3 in forged (left) and aged (right) conditions. Backscattered images from SEM (a) and (b) and TEM micro-graphs (c) and (d). The selected area diffraction pattern from the β matrix is shown in (c); streaking is observed between the β peaks.

The differences in bulk stress-strain behaviour and increase in strength of the aged sample compared to the forged can be attributed to differences in microstructure, Figure 4. The forged material shows a well-developed β subgrain structure with large globular primary α on the prior β grain boundaries and partially broken-up intraganular α laths between the subgrains. The aged sample also shows evidence of the spheroidisation of the primary α and precipitation of a on the β grain boundaries. In TEM, α precipitates around 20nm in width are observed within the β subgrain matrix. The composition of several of these was measured with X-EDS and they were found to contain only Ti and Al, whereas the β matrix contained Ti, Fe, V and small amounts of Al, as might be expected. Streaking was observed in the diffraction patterns of the β phase in the forged condition but the presence of ω could not be verified. It is anticipated that ω precipitates act as precursors to the fine scale α observed in the aged material[1].

4.2 The Response of the Lattice

Figure 5 shows the measured elastic lattice strain on selected peaks obtained from the diffraction spectra, with the unloads and reloads removed. In addition, the model predictions are shown, which are discussed later. Initially an elastic response is observed. After the onset of yielding, the elastic strain stops increasing in the weakest direction (or increases only due to hardening), and load partitions onto other unyielded orientations. Once macroscopic yielding of all orientations has occurred, the gradient of all the peaks returns towards that observed during elasticity. For example, in the forged sample in the longitudinal direction, the $\{10\bar{1}0\}$ oriented grains behave in an elastic manner until ~500MPa where yielding occurs. The load is then accommodated by the $\{10\bar{1}3\}$ oriented grains until 750MPa, approximately the same value as the macroscopic yield stress.

The aged material reaches higher elastic stresses than the forged, across all the grain orientations measured. The lattice strain graphs appear completely linear for all orientations

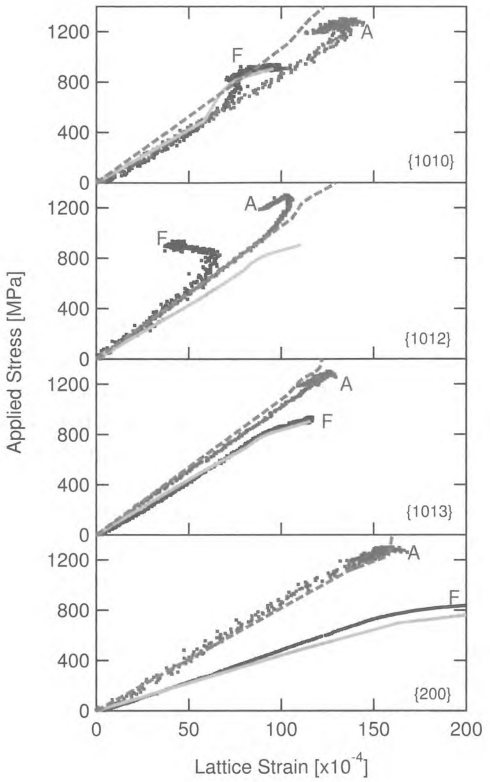

Figure 5. Applied stress *vs* lattice strain for differing peaks. F and A denote the Forged and Aged samples. The solid grey line shows the forged model prediction while the dashed grey line shows the prediction for the aged model.

Table 4. Diffraction elastic constants in the forged and aged conditions (GPa). The experimental and calculated model values are given, together with the ratio calculated/experimental, *c/e.*

Peak	Forged Stiffness			Aged Stiffness		
	e	c	c/e	e	c	c/e
$\{10\bar{1}0\}$	87	85	0.98	86	105	1.22
$\{10\bar{1}1\}$	-	-	-	110	97	0.88
$\{10\bar{1}2\}$	110	84	0.76	110	105	0.95
$\{10\bar{1}3\}$	87	86	0.99	87	86	0.99
{200}	45	44	0.90	88	82	0.93
{211}	-	-	-	93	97	1.04
{220}	70	71	0.98	-	-	-

until the $\{10\bar{1}2\}$ yields at around 900MPa. Mi-croscopic yielding is again substantially below the macro-scopic yield stress of 1100MPa.

4.3 Diffraction Elastic Constants

Table 4 shows the measured stiffness of the peaks derived from the elastic regime of the stress-lattice strain graphs. In the forged material, the $\{10\bar{1}2\}$ orientations appear the be the stiffest followed by the $\{10\bar{1}0\}$. The {200} β orientations are considerably more compliant with a stiffness in the {200} orientation of ~ 45GPa. The aged material shows similar stiffness values for the α orientations compared to the forged condition. However, an increased stiffness is observed in the {200} β orientation which increases from ~45GPa in the forged to ~88 GPa in the aged condition.

5. Discussion

5.1 Model comparison with experimental observations

The calculated response of the model for both the forged and aged conditions is shown in Figure 5 and in Table 4. There are some discrepancies with the stiffness predicted, but for 7 of the 9 DECs measured the model is within 12% of the experimental value.

For the forged sample, Figure 5, the model reproduces the observed behaviour very well for the $\{10\bar{1}3\}$ and $\{10\bar{1}0\}$ orientations. It predicts that the lattice strain should rise on deviation from linearity in the $\{10\bar{1}2\}$. In the β phase, data are only shown for the {200} orientation, where yielding is predicted at a lower stress level than indicated by the measurement. However, the trends in behaviour are reproduced.

In the model of the aged material, the $\{10\bar{1}3\}$ behaviour is again reproduced successfully. Similarly the yield point of the $\{10\bar{1}0\}$ and $\{10\bar{1}2\}$ is predicted correctly, but the drop in lattice strain on yielding is not predicted. In the β phase, however, the predictions appear to be very accurate for the {200} peak.

Given the complicated microstructure of the forged material, the model reproduces the lattice strain behaviour reasonably well. For the aged sample, reinforced with fine scale α precipitates, the model reproduces the behaviour of the β phase strikingly well, but the behaviour of the α is not reproduced as well. Since diffraction information is collected from both the primary and secondary α simultaneously, this is perhaps unsurprising.

5.2 Anisotropy of the β phase

Recent *ab initio* work[16] has suggested that $C_{11} - C_{12}$ approaches zero (at T = 0 K) for highly alloyed Ti-Nb-Zr-O. In the present work the measured diffraction elastic constants vary widely from those found using a model taking values taken from the literature, and also vary significantly between the two conditions (Table 2). The *ab initio* calculations correctly predict that pure *bcc* Ti has a negative $C_{11} - C_{12}$, *i.e.* it is unstable at absolute zero. $C_{11} - C_{12}$ is predicted to increase with β-stabiliser content (number of valence electrons), rendering the *bcc* phase stable. This is consistent with our measurements *i.e.* enriching the β in V and Fe increases $C_{11} - C_{12}$ and is also consistent with the single crystal constants fitted in the model.

5.3 Effect of fine scale α on the micromechanics of Ti-10-2-3

The magnitude of the load partitioning from the α to the β is smaller in the aged material compared to the forged condition. Notably, the CRSS for easiest slip in the α increases from 170MPa in the forged condition to 420MPa in the aged, whereas in the β easiest slip increases from 220MPa to 480MPa. Therefore in the forged condition the α deforms significantly before the β, but in the aged condition they both yield at approximately the same stress.

The major difference in the microstructure is the presence of fine scale α precipitates in the aged material. The increase in solid solution content in the β phase cannot readily explain the ~ 2 x increase in strength, or the simultaneous yield of the α. It seems likely that the majority of the increase in β strength observed is due to the inhibition of dislocation motion by the fine scale α in the aged material, and that the apparent yielding of the α is due to relaxation of the surrounding β and dislocation bypass.

6. Conclusions

The load partitioning between phases and grain orientations in both forged and aged Ti-10-2-3 has been investigated using synchrotron X-ray diffraction and a two-phase elastic-plastic self-consistent (EPSC) model. The following conclusions can be drawn from this work:

- The stiffness of the β phase in the {200} diffraction orientation increases from 45 to 88GPa between the forged and aged material. This is attributed to an increase in $C_{11} - C_{12}$ from 12 to 47GPa due to the increase in β-stabiliser content, in agreement with atomistic predictions.
- The EPSC models are reasonably successful at reproducing the observed behaviour, but do not provide a complete description of the micromechanics of these materials. This is expected, since the real microstructure is much more complex than the single-site interaction modelled.

Acknowledgements

SLR was funded by an EPSRC DTA studentship. The group is also supported by EPSRC platform grant GR/T26344/01. We would like to thank: Jeff Brooks at QinetiQ for material supply, Lee Semiatin at AFRL, Dayton OH, USA for forging the material, Andy Gotz and Magnus Bostrom at ESRF, Howard Stone at the Universities of Manchester and Cambridge and Ioannis Bantounas, Russell Talling and Mahmoud Ardakani for assistance with TEM.

REFERENCES

1) T. W. Duerig, J. C. Williams, Beta titanium alloys in the 1980s (1984) 19-67.

2) J. D. Eshelby, Proc. R. Soc. London, Ser. A A241 (1957) 376-396.

3) J. W. Hutchinson, Proc. R. Soc. London, Ser. A A319 (1970) 247-272.

4) R. A. Lebensohn, C. N. Tomé, Acta Metall. Mater. 41 (9) (1993) 2611-2624.

5) D. Dye, H. J. Stone, R. C. Reed, Curr. Opin. Mater. Sci. 5 (2001) 31-37.

6) U. F. Kocks, C. N. Tomé, H. R. Wenk, Texture and Anisotropy, Cambridge University Press, Cambridge, UK (1998).

7) D. Dye, H. J. Stone, R. C. Reed, Acta Mater. 49 (2001) 1271-1283.

8) M. Jackson, R. J. Dashwood, H. M. Flower, L. Christodoulou, Mater. Sci. Technol. 16 (11) (2000) 1437-1444.

9) P. Turner, N. Christodoulou, C. N. Tomé, Int. J. Plast. 11 (3) (1995) 251-265.

10) R. Hill, J. Mech. Phys. Solids 15 (1967) 79-95.

11) W. Petry, A. Heimig, J. Trampenau, M. Alba, C. Herzig, H. Schrober, G. Vogl, Phys. Rev. B 43 (1991) 10933-10947.

12) B. A. Brandes, C. B. Brook, Smithells Metal Reference Book (1992).

13) E. S. Fisher, D. Dever, The Science, Technology and Applications of Titanium (1970).

14) H. Ledbetter, H. Ogi, S. Kim, M. Hirao, J. Appl. Phys. 95 (9) (2004) 4642-4644.

15) J. C. Williams, R. Baggerly, N. Paton, Metall. Trans. A 33A (3A) (2002) 837- 850.

16) H. Ikehata, N. Nagasako, T. Furuta, A. Fukumoto, K. Miwa, T. Saito, Phys. Rev. B 70 f(2004) 174113-1174113-8.